Accepted Manuscript

Preparation and characterization of lotus seed starch-fatty acid complexes formed by microfluidization

Bingyan Chen, Zebin Guo, Song Miao, Shaoxiao Zeng, Xiangze Jia, Yi Zhang, Baodong Zheng

PII:	S0260-8774(18)30223-1
DOI:	10.1016/j.jfoodeng.2018.05.020
Reference:	JFOE 9264
To appear in:	*Journal of Food Engineering*
Received Date:	22 November 2017
Accepted Date:	22 May 2018

Please cite this article as: Bingyan Chen, Zebin Guo, Song Miao, Shaoxiao Zeng, Xiangze Jia, Yi Zhang, Baodong Zheng, Preparation and characterization of lotus seed starch-fatty acid complexes formed by microfluidization, *Journal of Food Engineering* (2018), doi: 10.1016/j.jfoodeng.2018.05.020

Preparation and characterization of lotus seed starch-fatty acid complexes formed by microfluidization

Abbreviated running title: The characterization of lotus seed starch-fatty acid complexes

Bingyan Chen [a,b,d], Zebin Guo [a,b], Song Miao [c,a,d], Shaoxiao Zeng [a,b], Xiangze Jia [a,b], Yi Zhang [a,b,d], Baodong Zheng [a,b,d,*]

[a] *College of Food Science, Fujian Agriculture and Forestry University, Fuzhou, Fujian 350002, China*

[b] *Fujian Province Key Laboratory of Quality Science and Processing Technology in Special Starch, Fujian Agriculture and Forestry University, Fuzhou 350002, China*

[c] *Teagasc Food Research Centre, Moorepark, Fermoy, Co. Cork, Ireland*

[d] *China-Ireland international Cooperation Centre for Food Material Science and Structure Design, Fujian Agriculture and Forestry University, Fuzhou, Fujian 350002, China*

*Corresponding author:

(B. Zheng), College of Food Science, Fujian Agriculture and Forestry University, No.15 Shangxiadian Road, Cangshan District, Fuzhou City, Fujian Province, China.

E-mail address: zbdfst@163.com

Abstract: Using dynamic high pressure microfluidization, we prepared starch-lipid complexes from lotus seed starch (LS) and six saturated fatty acids (FAs) of different carbon chain length and analyzed their semi-crystalline structure and digestibility. Iodine blue value analysis showed the highest complex index (86.3%) was observed between LS and octanoic acid (C8). X-ray diffraction analysis showed crystal structure changed from V_{6II} to V_{6I} type with decreasing FA chain length. Small angle x-ray scattering and differential scanning calorimetry analyses confirmed the presence of a strong V_{6I}-type mass fractal structure with a Bragg distance of 12.3 nm in LS-C8, which can be considered to be a type-II complex with high melting temperature (T_p=123.98^{o}C). Scanning electron microscopy results showed the complexes had more spherocrystals with decreasing FA chain length. Compared to other FAs, C8 significantly reduced the LS susceptibility to digestive enzymes, increased slowly digestion starch content (26.06%) and decreased digestion rate (3.59×10^{-2}).

Keywords: lotus seed; fatty acids; carbon chain length; high pressure homogenization; crystalline structure; starch digestion in vitro..

1 Introduction

Lotus (*Nelumbo nucifera Gaertn*.) is a crop that has been cultivated for thousands of years in Asia including China, Japan, and India (Ming et al., 2013). In China, lotus is mainly harvested from July to September, and almost all parts of the lotus plant, including its seeds, leaves, pods, and rhizomes are used. The most common lotus part that is used in food products is the seed, which is a source of protein, vitamins, and minerals (Mukherjee et al., 2009). Lotus seeds, which have high antioxidant activity, can be processed into several food products including fried chips, pudding, biscuits, juice, beverages, and canned foods (Cai et al., 2008). However, the major component of lotus seed is starch (70% dry weight) (Zhang et al., 2013). Lotus seed has strong glycemic response after consumption and has limited edible potential of obesity and diabetes. Therefore, decreasing the digestion rate of lotus seed starch has become an area of significant interest among researchers.

Several studies have reported that fatty acids decrease the digestive rate of starch. During heated gelatinization, amylose forms helical complexes with fatty acids. Hydrogen bonds and hydrophobic interactions are considered to be the driving forces in the helical conformation (Karkalas et al., 1995; López et al., 2012). Upon cooling, these helical complexes can further stack into V-type crystalline complexes, which have a low susceptibility to digestive enzymes (Ai et al., 2013; Okumus et al., 2017), The digestibility of V-type complexes is affected by the amount and type of fatty acid. Tang and Copeland (2007) observed that the amount of fatty acids was highly correlated to the complex index of amylose-fatty acid complexes, which determine anti-enzymatic hydrolysis ability of starch. Fatty acids with long carbon chains form more enzyme-resistant complexes, while unsaturated fatty acids interfere with the formation of V-type complexes (Annor et al., 2015). According to Vasiliadou

et al. (2015), V-type complexes can be formed on the surface or inner cavity of starch granules during controlled heating conditions. The formation of enzyme-resistant V-type complexes is dependent on the temperature of preparation.

In recent years, non-thermal processing have been widely used in food industry (Amaral et al., 2017; Cappato et al., 2018). Non-thermal starch modification, e.g., via enzyme addition (Cheng et al., 2015), alkali addition (Putseys et al., 2010), or mechanical methods (Bail et al., 2013; Kong and Ziegler, 2014), has been used to improve the slowly digestible properties of complexes. However，these technologies are expensive and not environmentally friendly, which limits their applications in food industrial processes. Dynamic high pressure microfluidization (DHPM) is novel technology that has been extensively applied in the chemical and pharmaceutical industries. In DHPM, liquid carrying solid particles is subjected to ultra-high shear pressure (200 MPa) for a short period of time (less than 3s) in a micro-channel interaction chamber. DHPM reduces the molecular weight of polymers and reorganizes macromolecules (Liu et al., 2009). The schematic diagram of DHPM is shown in Fig.1. Modified starch may be more suitable for the formation of starch-fatty acid complexes due to a high proportion of linear starch chains. DHPM is performed at ambient temperature to prevent damage to heat-sensitive molecules. Additionally, there are no organic solvents in DHPM, making this method suitable for the food industry. Currently, the application of DHPM in food research is mainly focused on the interactions between proteins and non-starch polysaccharides and between proteins and cellulose (Chen et al., 2013; Liu et al., 2016). However, to the best of our knowledge, no study has focused on the use of DHPM for the preparation of starch-fatty acid complexes.

In this study, the starch-fatty acid complexes were prepared using lotus seed

starch (LS) and fatty acids (FAs) of different carbon chain length via DHPM. Additionally, the changes in morphology and crystalline structure of LS-FA complexes were evaluated. The structure and morphology of these complexes were characterized using wide angle X-ray diffraction (XRD), small angle X-ray scattering (SAXS), differential scanning calorimetry (DSC), and field-emission scanning electron microscopy (FESEM). Furthermore, digestible properties of LS-FA complexes were studied using digestion curves and enzyme kinetics parameters.

2 Materials and methods

2.1 Materials

LS with an amylose/amylopectin ratio of 45/55 was obtained from Green Field Food Co., Ltd. (Fujian, China), defatted with ethanol, and dried in an air oven at 40 ± 1°C for 16 h. Octanoic acid (C8:0), decanoic acid (C10:0), lauric acid (C12:0), myristic acid (C14:0), palmitic acid (C16:0), and stearic acid (C18:0; purity 99%) were purchased from Merck Chemical Co., Ltd (Darmstadt, Germany). α-Amylase from porcine pancreas (≥ 50 units mg^{-1} protein) and amyloglucosidase from *Aspergillus niger* (≥ 260 unit mL^{-1}) were supplied by Sigma-Aldrich Co Ltd., USA. All other chemicals were of analytical grade.

2.2 Formation of LS-FA complexes by DHPM

Each FA (0.1 g, 5%, w/w, dry starch base) was dissolved in 50% ethanol and mixed with the defatted LS slurry (2 g, 4%, w/w). The mixed solution was subjected to DHPM eight times at 200 MPa in a SPCH-EP-IC-16-30 microfluidizer (STANSTED Co., London, England). When homogenized cycle number is 8 time, the complex index of all samples reached the maximum according to the optimization conducted previously. The instrument was equipped with one interaction chamber of 75 μm in diameter. A cooling water circulating pump connected to a interaction

chamber was used to prevent severe heat damage to the samples and guarantee the temperature effect to be minimal. After homogenization, the temperature of mixed solution was measured using a electronic thermometer. The temperature of all the samples was not more than 35°C. Part of the mixed solution was used to determine complex index (CI), while another part was freeze-dried for structure analysis.

2.3 Iodine-blue measurement

CI was determined by the iodine blue method (Kaur and Singh, 2000). The starch dispersion was heated to 100℃ for 15 min and centrifuged at 3,500 g for 10 min. An aliquot of the resulting supernatant (50 μL) was mixed with 4 mL of iodine (0.1% I_2, w/w and 2% KI w/w in deionized water) and gently vortexed. The absorbance (ABS) values of the sample and reference (devoid of FAs) were measured at 690 nm. CI was calculated using the following equation (Eq. 1),

$$CI = 100 \times \left(ABS_{\text{reference}} - ABS_{\text{sample}} \right) / ABS_{\text{reference}} \quad (1)$$

2.4 X-ray diffraction (XRD)

XRD analysis of LS-FA complexes was carried out using a D/MAX 2200PC X-ray diffractometer (Rigaku Corporation, Tokyo, Japan). X-ray diffraction patterns were obtained between 0-35° 2θ at a scanning speed of 8° /min. Relative crystallinity was measured as the area ratio of the crystalline sharp peak over the total area using Jade 6.0 software.

2.5 Small-angle X-ray scattering (SAXS)

LS-FA complexes were dispersed in excess water, and the starch suspensions (40% wt) were placed on multi-well stage and then performed on a Bruker NanoStar SAXS instrument. The parameters of the SAXS spectrum were determined by the method reported by (Cai et al., 2014) with some modifications. The date in the angular range of $0.007 < q < 0.23 Å^{-1}$ were used as the SAXS pattern, where q =

136 $4\pi\sin\theta/\lambda$. The data were background subtracted and normalized.

137 *2.6 Differential scanning calorimetry (DSC)*

138 The thermal behaviors of LS-FA complexes were measured using a differential
139 scanning calorimeter (DSC-200FC, NETZSCH, Selb, Germany). A high-pressure
140 stainless steel pan with a gold-plated copper seal was used to run the tests. Samples (3
141 mg) were weighed into stainless steel pan and each pan was hermetically sealed after
142 addition of 7 μL distilled water using a micro-syringe. The samples were prepared to
143 stand at 25°C for 12h, and then were heated from 25°C to 150°C at a heating rate of
144 10°C/min. A sealed empty pan was used as a reference. The gelatinization onset
145 temperature (T_o), peak temperature (T_p), end temperature (T_e), and enthalpy (ΔH) of
146 the starch samples were recorded by Netzsch software.. All results were reported as
147 averages of three replicates.

148 *2.7 Scanning electron microscopy*

149 Samples were mounted on aluminum stubs with sticky double-side carbon tape.
150 Excess powder was removed using high-pressure air. Samples were coated with gold
151 palladium by a mini sputter coater (Quorum SC7620; Quorum Technologies Ltd,
152 Laughton, UK). The morphology of LS-FA complexes was observed under an
153 emission scanning electron microscope (JSM-6360LV, JEOL, Tokyo, Japan) in low
154 vacuum mode at an accelerating voltage of 30 keV. The magnification of image was
155 10,000×.

156 *2.8 In vitro digestion*

157 In vitro digestion of LS-FA complexes was performed as reported by Zeng et al.
158 (2016) with a minor modification. Freeze-dried starch samples (300 mg, dry basis)
159 were dispersed in 5 mL of distilled water and heated to 100°C for 15 min. After
160 cooling to 37°C in a water bath, enzyme solution (1,500 unit mL^{-1} α-amylase, 0.1 M

161 sodium phosphate buffer, pH 6.5, 0.01% NaN_3, and 2.5 mM $CaCl_2$) was added and
162 shaken (100 rpm) at 37°C in a water bath. Within 0 and 180 min, an aliquot of the
163 digest (1 mL) was collected and heated in boiling water to terminate the reaction. The
164 digest was subsequently mixed with sodium acetate buffer (3 mL, 0.4 M, pH 4.6),
165 amyloglucosidase (≥ 260 unit mL^{-1}, 1 mL), and incubated in a water bath at 50°C for
166 45 min. Glucose concentration (GC) was determined in triplicate using the 3,5-
167 dinitrosalicylic acid (DNS) method at 540 nm. The glucose could be translated into
168 starch through dehydration condensation, namely the molecule weight (180) of
169 glucose subtracts a water molecule (18). Hence, the content of hydrolyzed starch was
170 calculated using a CG conversion factor of 0.9. The percentage of rapidly digestible
171 starch (RDS), slowly digestible starch (SDS), and resistant starch (RS) was calculated
172 from the following equations (Eq. 2),

$$RDS\ (\%) = \left[(G_{20} - FG)/TS\right] \times 0.9 \times 100$$

173 $$SDS\ (\%) = \left[(G_{120} - G_{20})/TS\right] \times 0.9 \times 100$$

$$RS\ (\%) = \left[(TS\text{-}G_{120})/TS\right] \times 0.9 \times 100 \quad (2)$$

174 where G20 and G120 represent the glucose amount released at 20 and 120 min of
175 hydrolysis, respectively, FG is the amount of free glucose in starch, and TS is total
176 starch weight.

177 *2.9 First-order kinetics*

178 To describe the digestion rate of LS-FA complexes, a first order kinetic model
179 (Eq. 3) was used to fit the digestion data.

180 $$C_t = C_\infty \left(1\text{-}e^{-kt}\right) \quad (3)$$

181 The Formula (Eq.3) can be transformed into a linear equation (Eq. 4)

182 $$\ln\left(\frac{C_\infty - C_t}{C_\infty}\right) = kt \quad (4)$$

where C_t (%) is the amount of starch digested at a given time (t min), C_∞ (%) is the estimated percentage of starch digested at the end point, and *k* is the coefficient of starch digestion rate. The value of k can be obtained from the slope of the linear-least-squares fit of $\ln\left(\frac{C_\infty - C_t}{C_\infty}\right)$ against t.

2.10 Statistical analysis

Graphs were generated using Origin Pro 8.5. The data were expressed as mean values and standard deviations. Data were analyzed by ANOVA and LSD test ($p < 0.05$) using the DPS 9.05 Statistical Software Program (Science Press, Beijing, China). All data are account to one decimal places.

3 Results and discussion

3.1 Complex index (CI)

CI is based on the formation of starch-iodine complexes in a starch-FA system; therefore, CI is indicative of the degree of starch that is complexed to FAs. The more starch-fatty complexes, the weaker the blue intensity in the supernatant. Figure 2 shows the CI values and supernatant images of several starch-FA complexes prepared by DHPM. The CI values of LS-C18 and LS-C16 were 11.8% and 12.8%, respectively, with no obvious color differences between them. The CI values of these complexes increased with decreasing FA chain length, reaching a maximum of 86.3% in LS-C8, which stained orange. Similar results were also reported in previous study (Kawai et al., 2012), which indicated that short chain FAs are better dispersed in a starch matrix compared to long chain FAs, thereby facilitating their interactions with amylose and the formation of more complexes. Meng et al. (2014) observed that high pressure homogenization promotes the formation of amylose-FA complexes. At 100 MPa, the CI values of amylose-C18 and amylose-C16 were 54.6% and 59.8%,

207 respectively. However, the weak complexing ability of LS-C18 and LS-C16 obtained
208 by DHPM could be attributed to the fact that DHPM (200 MPa) decreased the chain
209 length of amylose, thereby limiting the incorporation of long chain FAs in the helical
210 cavity. Changes in starch chain length following DHPM have been confirmed by Tu
211 et al. (2010), who reported that the structure of starch was fractured at 160 MPa.

212 *3.2 Wide-angle X-ray diffraction*

213 Figure 3 shows the diffraction pattern of LS and various LS-FA complexes
214 prepared by DPHM. LS exhibited four reflections (2θ) at 15°, 17°, 18°, and 22° and a
215 weaker peak at 26°, confirming its C-type crystalline structure (Zhang et al., 2014).
216 The intensity of these peaks decreased, and diffuse LS diffraction patterns were
217 observed following DPHM, indicating the loss of the C-type crystalline structure. In
218 contrast, Choi et al. (2009) and Xia et al. (2015) reported no noticeable shifts or
219 changes in the X-ray diffraction patterns of corn starch and tapioca starch following
220 high pressure shearing at 200 MPa. Therefore, the crystalline structure of LS might be
221 more susceptible to high pressure than corn starch and tapioca starch. When fatty
222 acids were added to starch system in DPHM treatment, two additional peaks at 21.7°
223 and 24.1°, which showed a typical V_{6II}-type crystal structure, was obtained in the
224 spectra of LS-stearic acid (C18), LS-palmitic acid (C16), and LS-myristic acid (C14).
225 However, the spectra of LS-C12, LS-C10, and LS-C8 had only three strong peaks at
226 7°, 13°, 20°, which are characteristic of V_{6I}-type inclusion conformations with six
227 glucose units per turn (Lesmes et al., 2009). Marinopoulou et al. (2016b) obtained two
228 additional peaks (21.7° and 24.1°) due to physically trapped free FA crystals between
229 helices in the crystalline complexes. These results suggested that long chain FAs are
230 not suitable to interact with starch chains during DHPM. Long chain FAs have low
231 solubility in aqueous phase and have the ability to reorganize themselves into

micelles, which adhere to complex helices and are difficult to remove by ethanol-water solution. The X-ray diffraction patterns that we obtained were in agreement with the CI results, further confirming the weak complexing ability of long chain FAs. Furthermore, the crystallinity of these complexes was independent on the carbon chain length of FAs. LS-C18 and LS-C16 exhibited lower degree of crystallinity (21.4% and 20.9%, respectively) than other complexes, presumably due to the fact that these entrapped free FA crystals hindered the arrangement of inclusion complexes between each other and contributed to an amorphous stacking of individual lamellar structures during the growth process. The highest degree of crystallinity (48.2%) was observed with LS-C8, indicating that the aggregation of these helices into dense semi-crystalline structures occurred with decreasing FA carbon chain length.

3.3 SAXS analysis

A nanoscale characterization of various starch-FA complexes ($0.1^o < 2\theta < 3.2^o$) was performed using SAXS (Fig. 4). LS showed one obvious characteristic peak at q = 0.63/nm, which corresponds to a lamellar structure with a Bragg distance of 9.97 nm according to $d = 2\pi/q$. This lamellar structure may originate from the radial orientation of amylopectin molecules, which can assemble into concentric regions of alternating amorphous and crystalline structures known as growth rings (Cameron and Donald, 1993). Following DHPM treatment, a distinct peak located at q = 0.63/nm disappeared, indicating that the semi-crystalline structure of LS was damaged by strong collision and high pressure. Moreover, LS-C8 showed an obvious shoulder peak at q = 0.51/nm, which was not present in LS-C18, LS-C16, or LS-C14. This result suggests that short chain FAs affect the nanoscale of complexes and that an ordered structure with a Bragg distance of approximately 12.3 nm was present in

these V_6-type complexes. Similar results were obtained by Zabar et al. (2009), who reported that V-type amylose-C12 complexes showed a typical nanostructure with a Bragg distance of 12.5 nm. In contrast, HernáNdezhernáNdez et al. (2011) and Shogren et al. (2006) reported that birefringence and lamellar thickness of 7.5–10 nm appeared in adjacent crystalline layers of complexes prepared by jet cooking. Chen et al.(2015) reported that a semicrystalline structure with a Bragg distance of 19.04 nm formed between debranched-starch and phosphatidylcholine. Therefore, the nanoscale characterization of starch-FA complexes is inconclusive. The nanoscale characteristics of starch-FA complexes are likely influenced by processing methods.

The fractal structure of various starch-FA complexes can be characterized by fractal dimension D, which indicates the compactness of a system. This can be achieved from the scattering power law equation (Eq. 5)

$$I(q) \propto q^{-a} \tag{5}$$

where I is the scattering intensity, and α is an exponent that ranges between 1 to 4 and that can be obtained from the slope between log I and log q. For example, $D_m = a$ ($1 < \alpha < 3$) indicates that the scattering objects can be interpreted as possessing a mass fractal structure, whereas $D_s = 6\text{-}a$ ($3 < \alpha < 4$) indicates that the object has an irregular surface and a surface fractal structure. As shown in Fig. 4, LS had an obvious mass fractal structure with $D_m = a = 2.9$, suggesting that the LS granule had a self-similar nature. Compared to LS, DHPM-treated LS had higher a values, which suggests that the scattering object in the LS granule became more loose and irregular by jet collision and presented a surface fractal structure with $a = 3.1$ and $D_s = 2.9$. Moreover, all complexes displayed a mass fractal structure with D_m ranging from 2.5 to 1.9; the lowest D_m value was obtained with LS-C8. This result suggested that DHPM reassembled starch and FAs into a tightly arranged structure. LS-C8 exhibited

a more compact lamellar structure.

3.4 Thermal analysis

Starch complexes can be divided into less ordered type-I complexes and semi-crystalline type-II complexes. Type-I complexes result in the formation of randomly oriented helical segments and have melting temperatures < 105°C (Karkalas et al., 1995). To assess the relationship between semi-crystalline structures and thermodynamic states, we measured the transition temperatures and association enthalpies (ΔH) of various starch-FA complexes (Table 1A). LS showed one endothermic peak at 67.2–81.3°C, with an enthalpy of 2.9 J/g, that was attributed to the hydration of starch granules during gelatinization. The T_p and ΔH values of LS significantly decreased after DHPM treatment, further confirming that the crystalline structure of LS was disrupted by DHPM. Moreover, there were obvious discrepancies in the thermal properties of LS-FA complexes. In complexes containing C18, C16, and C14 there were two endothermic peaks. The first peak is attributed to the melting of the crystalline structure of FA, which was entrapped between helices of the crystalline complexes. The second peak is attributed to the dissociation of type-I complexes. However, LS-C12, LS-C10, and LS-C8 exhibited one endothermic peak with high melting temperatures (T_p = 109.4°C to 123.9°C), that are characteristic of type-II complexes.

Marinopoulou et al. (2016a) reported that V-amylose thermostability increases with increasing FA chain length and decreases with increasing degree of FA unsaturation. The authors attributed this phenomenon to an increase in the extent of hydrophobic interactions taking place inside the cavity of the amylose helix. Gelders et al (2005) found that long amylose chains with DP80-400 results in the formation of the amylose-decosanoic complexes melting at high temperature. However, different

idea was reported by Zhou et al (2013), who found that small amylose chain with DP 23-127 favored the formation of stable amylose inclusion crystals. These results suggested that the dissociation temperature of starch-fatty acid was determined together by fatty acid type and amylose chain length. Degraded starch chain was suitable to crystal complex with octanoic acid during DHPM treatment. The higher crystalline degree of complex formation, the higher the dissociation temperature and dissociation enthalpy.

3.5 Microscopy

To investigate the effect of different FAs on the morphology of LS following DHPM treatment, we observed the appearance of LS and LS-FA complexes by SEM (Fig. 5). LS granules were elongated and oval in shape with smooth surfaces. Following DHPM treatment, the starch granules began to lose their spherical structure, and deformed and collapsed granules were observed. This result indicated that DHPM causes severe disruption of LS by drastic collision and pressure interaction. Similar results were obtained with corn starch subjected to high pressure homogenization (Wei et al., 2017). LS-FA complexes had different morphologies depending on the type of FA. LS-C18 and LS-C16 had an amorphous layer phase with rough surfaces, whereas the addition of myristic acid (C14) resulted in the formation of spherocrystallites on the surface of the layer phase. This result was agreement with the SEM image of previous studies (Fanta et al., 2008; Vasiliadou et al., 2015), which ascribed these protruded crystalline structures to the presence of amylose-lipid complexes. Moreover, the amorphous layer phase disappeared with decreasing FA chain length, and a large number of small spherulites were adhered to each other in the image of LS-C12 and LS-C10. These spherulites could be closely aggregated in parallel to each other; a more ordered lamellar morphology was evident

in LS-C8. According to the Fanta and Felker (2006), the morphology of complexes is largely influenced by fatty acid structure, fatty acid yielded from torus/disc species to spherical/lobed particles with the decrease of fatty acid chain length. Bhosale and Ziegler (2010) reported that the morphology of complexes is hardly influenced by temperature, but can be affected by the cooling rate during complex formation. Cooling rate significantly determines the size of spherulites. In our SEM images, short FAs were more favorable for the formation of LS-FA complexes and generated spherocrystals following DHPM treatment. For LS-C8, these spherocrystals have the capacity of arranging and forming a more compact lamellar morphology. However, it is necessary to further confirm these spherocrystals are formed either in homogeneity or in cooling process. These results were consistent with the results obtained from SAXS, which revealed a strong mass fractal structure in LS-C8.

3.6 Digestibility analysis

Figure 6 shows the digestibility of LS and various LS-FA complexes prepared by DHPM. LS displayed a high hydrolysis degree after 60 min of digestion due to the heat-induced swelling of the starch amorphous structure. After 60 min, the hydrolysis degree of LS treated by DHPM was higher than that of LS, indicating that the disruption of the crystalline and unfolded granule structure contributed to the exposure of more binding sites for enzymes. The hydrolysis degree of LS and LS-DHPM remained constant as the time was further increased to 180min. The digestibility of LS was affected by the type of FA. There were no obvious differences among LS, LS-C18, and LS-C16 in hydrolysis degree, whereas hydrolysis decreased in LS-C14, LS-C12, LS-C10, and LS-C8. LS-C8 had the lowest hydrolysis degree (70.32%) after 180 min of digestion.

The digestion rate of various starch-FA complexes can be described by the

kinetic profiles (LOS) of in vitro digestion. All starch samples closely followed first-order behavior according to the R values (0.991–0.996) obtained; therefore, LOS may accurately describe the starch digestion process. The digestion rate (*k*) of LS-C18 and LS-C16 was similar to that of LS, whereas LS-C8 had the lowest *k* value. This result can be attributed to the changes in nutritional starch fractions (RDS, SDS, and RS) as reported by Shu et al. (2009). The authors observed that SDS and RS were associated with low digestion rates. The changes in nutritional starch fractions are presented in Table 1b. RDS, SDS, and RS fractions in LS were 72.4%, 14.1%, and 13.5%, respectively. RDS content was lower in LS than in DHPM-treated LS. However, the RDS content of complexes decreased with decreasing FA chain length. LS-C8 had an RDS content of 30.2%, an SDS content of 40.1%, and a RS content of 28.6%. These results confirmed that more RDS was converted into SDS and RS in LS-C8, which reduced the digestibility of LS. In previous study, Okumus et al (2018) reported that fatty acid type was a determinant factor for starch hydrolysis. Stearic acid and palmitic acid additions applied with cooking significantly increased the SDS content in brown lentil starch; soy oil and olive oil additions resulted in deceases. However, Kawai et al (2012) found that the digestive properties of starch - fatty acid complexes was only dependent on complex index. This complex was related with the restrictedly swollen starch granules that reduced starch hydrolysis. In our study, high homogenized pressure (200MPa) disrupted starch granules, and C-type crystal structure disappeared in XRD pattern. Hence, the decline in enzymatic hydrolysis was mainly attributed to amylose-lipid complexes, which changed semi-crystalline structure of starch.

3.7 Relationship between digestibility and semi-crystalline structure

According to a previous study (Gelders et al., 2005), α-amylase resistance in

starch-lipid complexes increases with increasing lipid chain length due to lower solubility and higher steric hindrance. However, in our study, the digestibility of LS-FA was dependent on the semi-crystalline structure of the system. LS-C18 and LS-C16 had low CI following DHPM, leading to free stearic acid and palmitic acid being entrapped between the helices of starch chains instead of penetrating into the cavity of helices. This result was confirmed by the iodine blue test and XRD results. The changes in helical conformation resulted in the formation of imperfect semi-crystalline structures, which have lower transition temperatures and are type-I complexes based on DSC analysis. These amorphous type-I complexes fragments can be dissociated during gelatinization and have no obvious effects on the digestion rate of LS.

Complexes with short FA chain lengths had a high CI, especially in LS-C8. LS-C8 displayed a more heat-stable V_6-type lamellar crystal structure with a repeated unit distance of 12.3 nm. This result was confirmed by XRD, SAXS, and DSC analyses. These type-II complexes, which originate from the ordered stacking of spherocrystals, exhibited more compact lamellar morphology and decreased the accessibility of starch chains to digestive enzymes, thereby decreasing hydrolysis and reducing digestion rate. However, the molecule mechanism of formation of these slowly digestible semi-crystalline structure, which is formed during homogenization or during cooling by self-assembly needs further study. On the other hand, high pressure microfluidization has been considered to be able to reduce the particle size, which effect surface area and hydrophilic property of food material. Hence, the dispersity and solubility of these V_{6I} type complexes in aqueous phase will be needed to be performed in the future.

4 Conclusion

In this study, LS-FA complexes were synthesized by DHPM, their structure, morphology and digestibility properties were analyzed. The results showed that short chain FAs were suitable to interact with LS. The V-type polymorph in LS-FA complexes improved with decreasing FA chain length. The formation of a strong V_6-type semi-crystalline structure with a Bragg distance of 12.3 nm in LS-C8 was confirmed by XRD and SAXS. The LS-C8 complex had a high melting temperature and displayed a smooth and compact lamellar morphology, which probably originated from the ordered arrangement of spherocrystals during DHPM. Following the addition of C8, LS digestibility decreased due to the formation of a semi-crystalline lamellar structure that decreased the susceptibility to digestive enzymes. Although an external cooling system was used to make that temperature effect to be minimal, we cannot be 100% certain that internal momentary increases in temperature has not impact on the formation of starch-fatty acid complexes during rapid compression. This view needs to be studied in the future. However, this can still provide an effective method to prepared continuously slowly digestible starch by complexing with short chain fatty acid.

Acknowledgments

This study was financially supported by the National Natural Science Foundation of China (No. 31501485) and the Scientific and Technological Innovation Team Support Plan of Institution of Higher Learning in Fujian Province (Grant No. [2012]03). Furthermore, the study was supported by the Construction Projects of Top University (Grant No. 612014042) and the programme on Fujian Agriculture and Forestry University of doctoral students going aboard to be joint trained Grant No. 324-112110075).

Reference

Ai, Y., Hasjim, J., Jane, J.L., (2013). Effects of lipids on enzymatic hydrolysis and physical properties of starch. *Carbohydrate polymers,* 92(1), 120-127.

Amaral, G.V., Silva, E.K., Cavalcanti, R.N., Cpc, M., Lgzs, A., Moraes, J., Alvarenga, V.O., Guimarã£Es, J.T., Esmerino, E.A., Freitas, M.Q., (2017). Whey-grape juice drink processed by supercritical carbon dioxide technology: Physicochemical characteristics, bioactive compounds and volatile profile. *Food chemistry*, 239, 697-703.

Annor, G.A., Marcone, M., Corredig, M., Bertoft, E., Seetharaman, K., (2015). Effects of the amount and type of fatty acids present in millets on their in vitro starch digestibility and expected glycemic index (eGI). *Journal of Cereal Science,* 64(11), 76-81.

Bail, P.L., Chauvet, B., Simonin, H., Rondeau-Mouro, C., Pontoire, B., Carvalho, M.D., Le-Bail, A., (2013). Formation and stability of amylose ligand complexes formed by high pressure treatment. *Innovative Food Science & Emerging Technologies,* 18(18), 1-6.

Bhosale, R.G., Ziegler, G.R., (2010). Preparation of spherulites from amylose–palmitic acid complexes. *Carbohydrate polymers,* 80(1), 53-64.

Cai, H., Liao, S., Shi, Y., Wu, Y., Zou, Y., Chen, Z., Liu, X., (2008). Value in Using and Development of Lotus Product. *Academic Periodical of Farm Products Processing,* 34(3), 253-265.

454 Cai, J., Cai, C., Man, J., Yang, Y., Zhang, F., Wei, C., (2014). Crystalline and
455 structural properties of acid-modified lotus rhizome C-type starch.
456 *Carbohydrate polymers,* 102(1), 799-807.
457 Cameron, R.E., Donald, A.M., (1993). A small-angle x-ray scattering study of starch
458 gelatinization in excess and limiting water. *Journal of Polymer Science Part B*
459 *Polymer Physics,* 31(31), 1197-1203.
460 Cappato, L.P., Ferreira, M., Pires, R., Cavalcanti, R.N., Bisaggio, R.C., Freitas, M.Q.,
461 Silva, M.C., Cruz, A.G., (2018). Whey acerola-flavoured drink submitted
462 ohmic heating processing: Is there an optimal combination of the operational
463 parameters? *Food chemistry,* 245, 22-28.
464 Chen, J., Liang, R.H., Liu, W., Li, T., Liu, C.M., Wu, S.S., Wang, Z.J., (2013).
465 Pectic-oligosaccharides prepared by dynamic high-pressure microfluidization
466 and their in vitro fermentation properties. *Carbohydrate polymers,* 91(1), 175-
467 182.
468 Cheng, W., Luo, Z., Li, L., Fu, X., (2015). Preparation and characterization of
469 debranched-starch/phosphatidylcholine inclusion complexes. *Journal of*
470 *Agricultural & Food Chemistry,* 63(2), 634-641.
471 Choi, H.S., Kim, H.S., Park, C.S., Kim, B.Y., Baik, M.Y., (2009). Ultra high pressure
472 (UHP)-assisted acetylation of corn starch. *Carbohydrate polymers,* 78(4), 862-
473 868.

474 Fanta, G.F., Felker, F.C., Shogren, R.L., Salch, J.H., (2006). Effect of fatty acid
475 structure on the morphology of spherulites formed from jet cooked mixtures of
476 fatty acids and defatted cornstarch. *Carbohydrate polymers*, 66(1), 60-70.
477 Fanta, G.F., Felker, F.C., Shogren, R.L., Salch, J.H., (2008). Preparation of
478 spherulites from jet cooked mixtures of high amylose starch and fatty acids.
479 Effect of preparative conditions on spherulite morphology and yield.
480 *Carbohydrate polymers,* 71(2), 253-262.
481 Gelders, G.G., Duyck, J.P., Goesaert, H., Delcour, J.A., (2005). Enzyme and acid
482 resistance of amylose-lipid complexes differing in amylose chain length, lipid
483 and complexation temperature. *Carbohydrate polymers,* 60(3), 379-389.
484 HernáNdezhernáNdez, E., ÁVilaorta, C.A., Hsiao, B.S., Castrorosas, J.,
485 Gallegosinfante, J.A., Moralescastro, J., Ochoamartinez, L.A., Gomezaldapa,
486 C.A., (2011). Synchrotron X-ray scattering analysis of the interaction between
487 corn starch and an exogenous lipid during hydrothermal treatment. *Journal of*
488 *Cereal Science,* 54(1), 69-75.
489 Karkalas, J., Ma, S., Morrison, W.R., Pethrick, R.A., (1995). Some factors
490 determining the thermal properties of amylose inclusion complexes with fatty
491 acids. *Carbohydrate Research,* 268(2), 233-247.
492 Kaur, K., Singh, N., (2000). Amylose-lipid complex formation during cooking of rice
493 flour. *Food chemistry,* 71(4), 511-517.

494 Kawai, K., Takato, S., Sasaki, T., Kajiwara, K., (2012). Complex formation, thermal
495 properties, and in-vitro digestibility of gelatinized potato starch–fatty acid
496 mixtures. *Food Hydrocolloids,* 27(1), 228-234.
497 Kong, L., Ziegler, G.R., (2014). Formation of starch-guest inclusion complexes in
498 electrospun starch fibers. *Food Hydrocolloids,* 38(3), 211-219.
499 López, C.A., Vries, A.H.D., Marrink, S.J., (2012). Amylose folding under the
500 influence of lipids. *Carbohydrate Research,* 364(364C), 1-7.
501 Lesmes, U., Cohen, S.H., Shener, Y., Shimoni, E., (2009). Effects of long chain fatty
502 acid unsaturation on the structure and controlled release properties of amylose
503 complexes. *Food Hydrocolloids,* 23(3), 667-675.
504 Liu, C.M., Liang, R.H., Dai, T.T., Ye, J.P., Zeng, Z.C., Luo, S.J., Chen, J., (2016).
505 Effect of dynamic high pressure microfluidization modified insoluble dietary
506 fiber on gelatinization and rheology of rice starch. *Food Hydrocolloids,* 57,
507 55-61.
508 Liu, W., Liu, J., Xie, M., Liu, C., Liu, W., Wan, J., (2009). Characterization and
509 High-Pressure Microfluidization-Induced Activation of Polyphenoloxidase
510 from Chinese Pear (Pyrus pyrifolia Nakai). *Journal of Agricultural & Food*
511 *Chemistry,* 57(12), 5376-5380.
512 Marinopoulou, A., Papastergiadis, E., Raphaelides, S.N., (2016a). An investigation
513 into the structure, morphology and thermal properties of amylomaize starch-
514 fatty acid complexes prepared at different temperatures. *Food research*
515 *international,* 90, 111-120.

516 Marinopoulou, A., Papastergiadis, E., Raphaelides, S.N., Kontominas, M.G., (2016b).
517 Structural characterization and thermal properties of amylose- fatty acid
518 complexes prepared at different temperatures. *Food Hydrocolloids,* 58, 224-
519 234.
520 Meng, S., Ma, Y., Cui, J., Sun, D.W., (2014). Preparation of corn starch–fatty acid
521 complexes by high-pressure homogenization. *Starch-Stärke,* 66(9-10), 809-
522 817.
523 Ming, R., Vanburen, R., Liu, Y., Yang, M., Han, Y., Li, L.T., Zhang, Q., Kim, M.J.,
524 Schatz, M.C., Campbell, M., (2013). Genome of the long-living sacred lotus (
525 Nelumbo nucifera Gaertn.). *Genome Biology,* 14(5), R41.
526 Mukherjee, P.K., Mukherjee, D., Maji, A.K., Rai, S., Heinrich, M., (2009). The sacred
527 lotus (Nelumbo nucifera) - phytochemical and therapeutic profile. *Journal of*
528 *Pharmacy & Pharmacology,* 61(4), 407-422.
529 Okumus, B.N., Tacer-Caba, Z., Kahraman, K., Nilufer-Erdil, D., (2017). Resistant
530 Starch Type V Formation In Brown Lentil (Lens Culinaris Medikus) Starch
531 With Different Lipids/Fatty Acids. *Food chemistry,* 240, 550-558.
532 Putseys, J.A., Derde, L.J., Lamberts, L., Ostman, E., Björck, I.M., Delcour, J.A.,
533 (2010). Functionality of short chain amylose-lipid complexes in starch-water
534 systems and their impact on in vitro starch degradation. *Journal of*
535 *Agricultural & Food Chemistry,* 58(3), 1939-1945.

536 Shogren, R.L., Fanta, G.F., Felker, F.C., (2006). X-ray diffraction study of crystal
537 transformations in spherulitic amylose/lipid complexes from jet-cooked starch.
538 *Carbohydrate polymers,* 64(3), 444-451.
539 Shu, X., Jia, L., Ye, H., Li, C., Wu, D., (2009). Slow Digestion Properties of Rice
540 Different in Resistant Starch. *Journal of Agricultural & Food Chemistry,*
541 57(16), 7552-7559.
542 Tang, M.C., Copeland, L., (2007). Analysis of complexes between lipids and wheat
543 starch. *Carbohydrate polymers,* 67(1), 80-85.
544 Tu, Z.C., Zhu, X.M., Chen, G., Wang, H., Zhang, B., Huang, X.Q., Li, Z., (2010).
545 Effects of dynamic high-pressure microfluidization on the structure of waxy
546 rice starch. *Food & Fermentation Industries,* 30(3), 834-837.
547 Vasiliadou, E., Raphaelides, S.N., Papastergiadis, E., (2015). Effect of heating time
548 and temperature on partially gelatinized starch-fatty acid interactions. *LWT -*
549 *Food Science and Technology,* 60(2), 698-707.
550 Wei, B., Cai, C., Xu, B., Jin, Z., Tian, Y., (2017). Disruption and Molecule
551 Degradation of Waxy Maize Starch Granules during High Pressure
552 Homogenization Process. *Food chemistry,* 240, 165-173.
553 Xia, W., Wang, F., Li, J., Wei, X., Fu, T., Cui, L., Li, T., Liu, Y., (2015). Effect of
554 high speed jet on the physical properties of tapioca starch. Food
555 Hydrocolloids, 49, 35-41.

556 Zabar, S., Lesmes, U., Katz, I., Shimoni, E., Bianco-Peled, H., (2009). Studying
557 different dimensions of amylose–long chain fatty acid complexes: Molecular,
558 nano and micro level characteristics. Food Hydrocolloids, 23(7), 1918-1925.
559 Zeng, S., Chen, B., Zeng, H., Guo, Z., Lu, X., Zhang, Y., Zheng, B., (2016). Effect of
560 microwave irradiation on the physicochemical and digestive properties of
561 lotus seed starch. Journal of Agricultural & Food Chemistry, 64(12), 95-110.
562 Zhang, Y., Wang, Y., Zheng, B., Lu, X., Zhuang, W., (2013). The in vitro effects of
563 retrograded starch (resistant starch type 3) from lotus seed starch on the
564 proliferation of Bifidobacterium adolescentis. *Food & Function,* 4(11), 1609-
565 1616.
566 Zhang, Y., Zeng, H., Wang, Y., Zeng, S., Zheng, B., (2014). Structural characteristics
567 and crystalline properties of lotus seed resistant starch and its prebiotic effects.
568 *Food chemistry,* 155(19), 311-318.
569 Zhou, X., Wang, R., Zhang, Y., Yoo, S.H., Lim, S.T., (2013). Effects of amylose
570 chain length and heat treatment on amylose–glycerol monocaprate complex
571 formation. *Carbohydrate polymers,* 95(1), 227-232.

573 **Table 1 The thermal properties and digestible properties of LS-FA prepared by DHPM treatment.**

(A) The enthalpy change and crystallinity of LS-FA prepared by DHPM treatment

	Peak 1				Peak 2					
	T_0（℃）	T_p（℃）	T_e（℃）	ΔH (J/g)	T_0（℃）	T_p（℃）	T_e（℃）	ΔH (J/g)	ΔHr (J/g)	Crystallinity (%)
LS	67.2±0.1^{a}	73.03±0.1^{a}	81.3±0.1^{a}	2.9±0.1^{a}					2.9	42.1±0.1^{c}
LS-DHPM	66.2±0.4^{b}	70.13±0.1^{b}	80.1±0.1^{b}	2.1±0.1^{b}					2.1	21.2±0.1^{e}
LS-C18	58.3±0.1^{c}	61.12±0.3^{d}	64.4±0.2^{d}	1.3±0.1^{c}	79.3±0.1^{f}	82.4±0.1^{e}	85.7±0.2^{e}	0.8±0.1^{f}	2.1	21.4±0.4^{e}
LS-C16	54.3±0.3^{e}	59.34±0.1^{e}	62.5±0.1^{e}	1.0±0.1^{d}	78.0±0.1^{e}	81.5±0.1^{f}	85.4±0.1^{f}	1.0±0.1^{e}	2.0	20.9±0.4^{f}
LS-C14	57.5±0.1^{d}	62.03±0.1^{c}	66.8±0.1^{c}	0.8±0.1^{e}	81.4±0.1^{d}	84.3±0.1^{d}	88.9±0.1^{d}	1.7±0.1^{d}	2.5	38.1±0.2^{d}
LS-C12					103.4±0.4^{c}	112.6±0.2^{b}	121.4±0.2^{b}	3.1±0.1^{b}	3.1	44.2±0.1^{b}
LS-C10					104.2±0.1^{b}	109.4±0.1^{c}	118.4±0.1^{c}	3.1±0.1^{c}	3.1	42.4±0.4^{c}
LS-C8					115.1±0.2^{a}	123.9±0.2^{a}	128.0±0.1^{a}	3.4±0.1^{a}	3.4	48.2±0.4^{a}

(B) The digestive parameters of LS-FA prepared by DHPM treatment

	D_0 (%)	D_{180} (%)	k ($\times 10^{-2}$)	R^2	RDS (%)	SDS (%)	RS (%)
LS	5.9±0.3^{b}	86.5±0.2^{b}	5.5±0.1^{b}	0.993	72.4±0.9^{b}	14.1±0.2^{f}	13.5±0.7^{g}
LS-DHPM	7.4±0.3^{a}	94.2±0.2^{a}	7.1±0.2^{a}	0.996	79.3±0.5^{a}	13.1±0.6^{f}	5.8±0.4^{h}
LS-C18	3.5±0.3^{c}	84.9±0.2^{c}	5.5±0.2^{b}	0.996	69.4±0.2^{d}	15.5±0.3^{e}	15.1±0.2^{f}
LS-C16	1.9±0.2^{f}	83.5±0.4^{cd}	5.3±0.2^{b}	0.993	70.7±0.3^{c}	13.8±0.5^{f}	16.6±0.2^{e}
LS-C14	3.2±0.1^{d}	82.4±0.6^{d}	2.9±0.2^{c}	0.992	50.1±0.2^{e}	32.4±0.4^{d}	17.7±0.2^{d}
LS-C12	2.9±0.1^{d}	79.3±1.3^{e}	2.1±0.1^{d}	0.995	46.0±0.2^{f}	34.4±0.2^{c}	20.6±0.2^{c}

LS-C10	2.9±0.3[d]	77.5±1.0[f]	2.2±0.1[d]	0.993	40.3±0.3[g]	37.2±1.1[b]	22.5±0.3[b]
LS-C8	2.3±0.1[e]	71.4±0.8[g]	1.9±0.1[e]	0.991	30.2±0.2[h]	40.1±0.4[a]	28.6±0.3[a]

574 Experimental data are the means of duplicates. Values followed by the same superscript letter within a column do not differ significantly ($P < 0.05$),

575 All data is account to one decimal places.

576

577

578

579

580

581

582

583

584

585

586

587

588

589

590 **Figure Caption**

591 Fig.1 The schematic diagram of dynamic high pressure microfluidization during the
592 experiment.

593 Fig.2 The complex index of lotus seed starch-fatty acids complexes prepared by
594 dynamic high pressure microfluidization at 200MPa

595 Fig.3 The XRD patterns of lotus seed starch-fatty acids complexes prepared by
596 dynamic high pressure microfluidization at 200MPa

597 Fig.4 The SAXS patterns of lotus seed starch-fatty acids complexes prepared by
598 dynamic high pressure microfluidization at 200MPa

599 Fig.5 The SEM image of lotus seed starch-fatty acids complexes prepared by dynamic
600 high pressure microfluidization at 200MPa. (a) LS (5000×); (b) DHPM-LS (5000×);
601 (A) LS (10000×); (B) DHPM-LS (10000×); (C) LS-C18 (10000×); (D) LS-C16
602 (10000×); (E) LS-C14 (10000×); (F) LS-C12 (10000×); (G) LS-C10 (10000×); (H)
603 LS-C8 (10000×).

604 Fig.6 The digestion profile (A) and LOS fit curves (B) of lotus seed starch-fatty acids
605 complexes prepared by dynamic high pressure microfluidization at 200MPa. ○,
606 Experiment data; □ , LOS plot data.

607 Figure 1

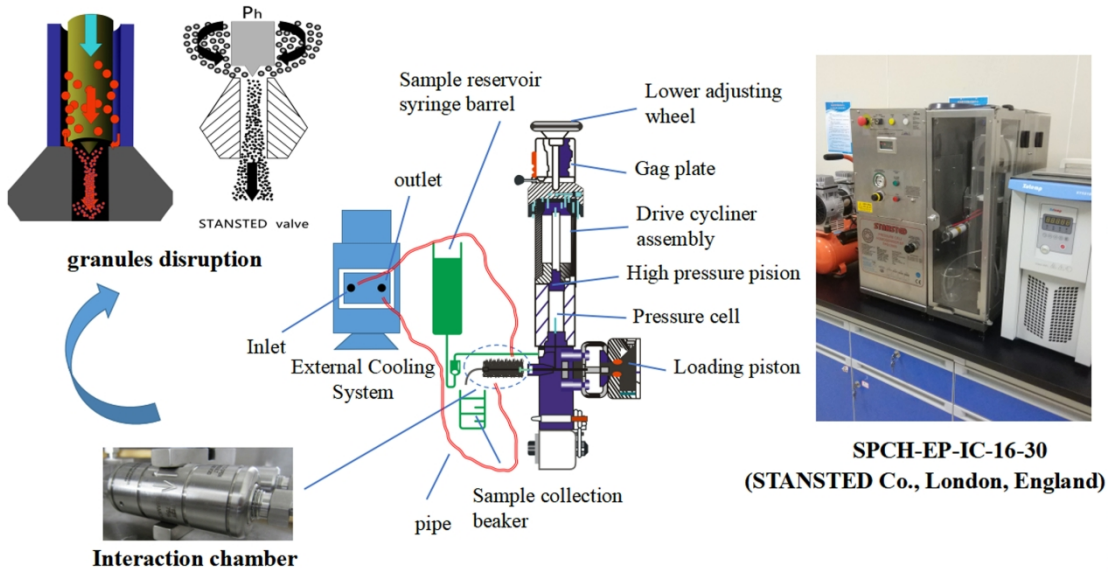

608

609 Figure 2

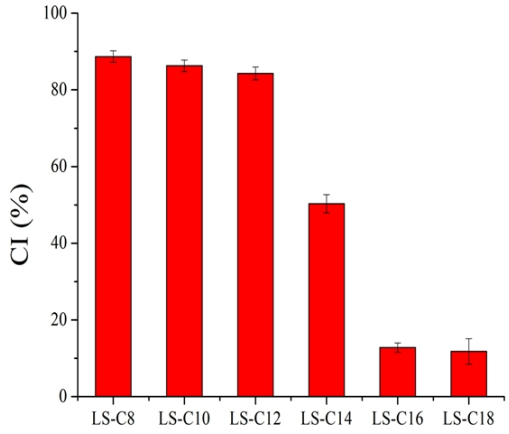

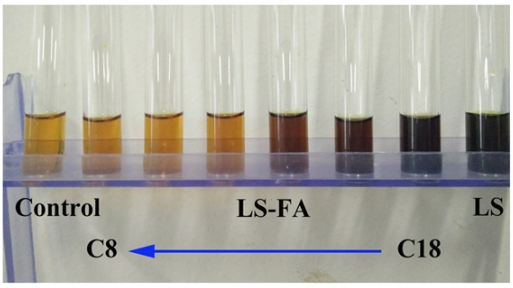

610

611 Figure 3

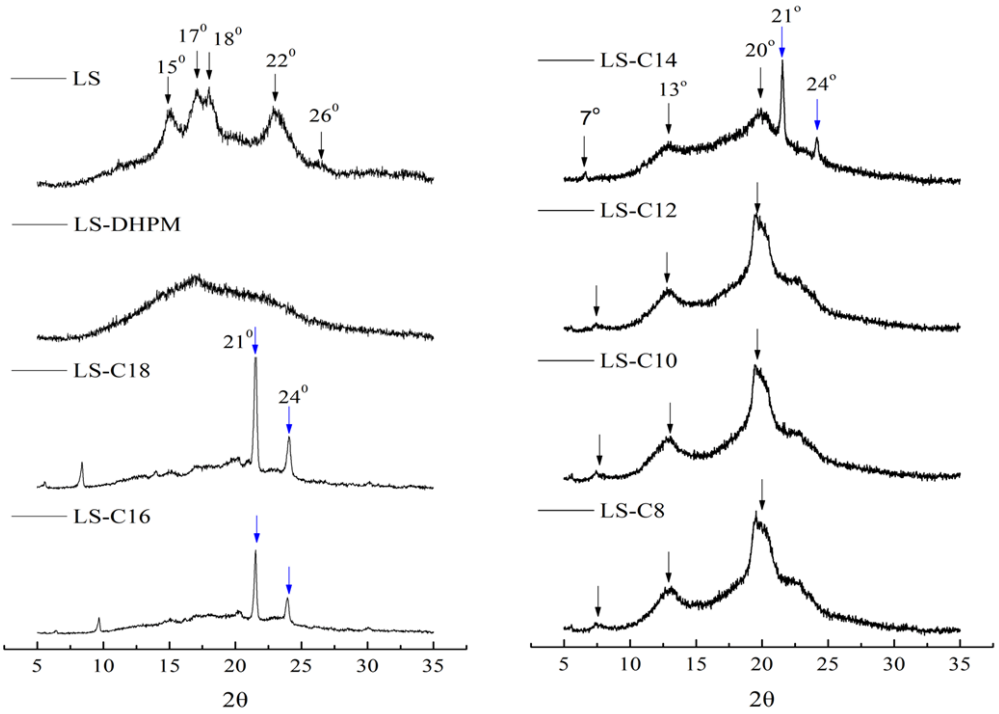

612

613 Figure 4

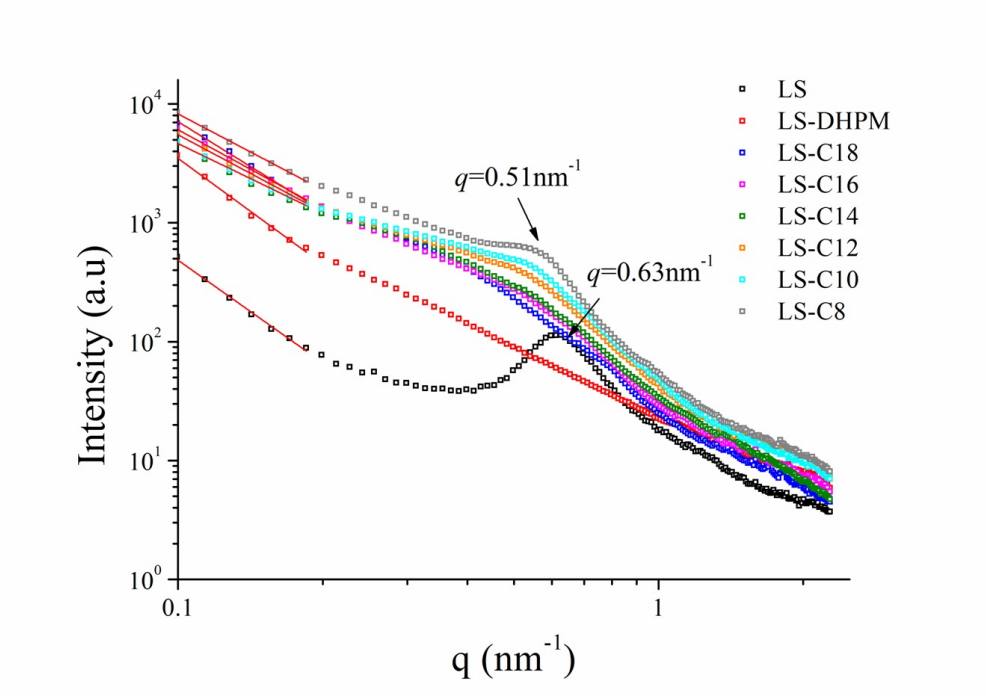

614

615 Figure 5

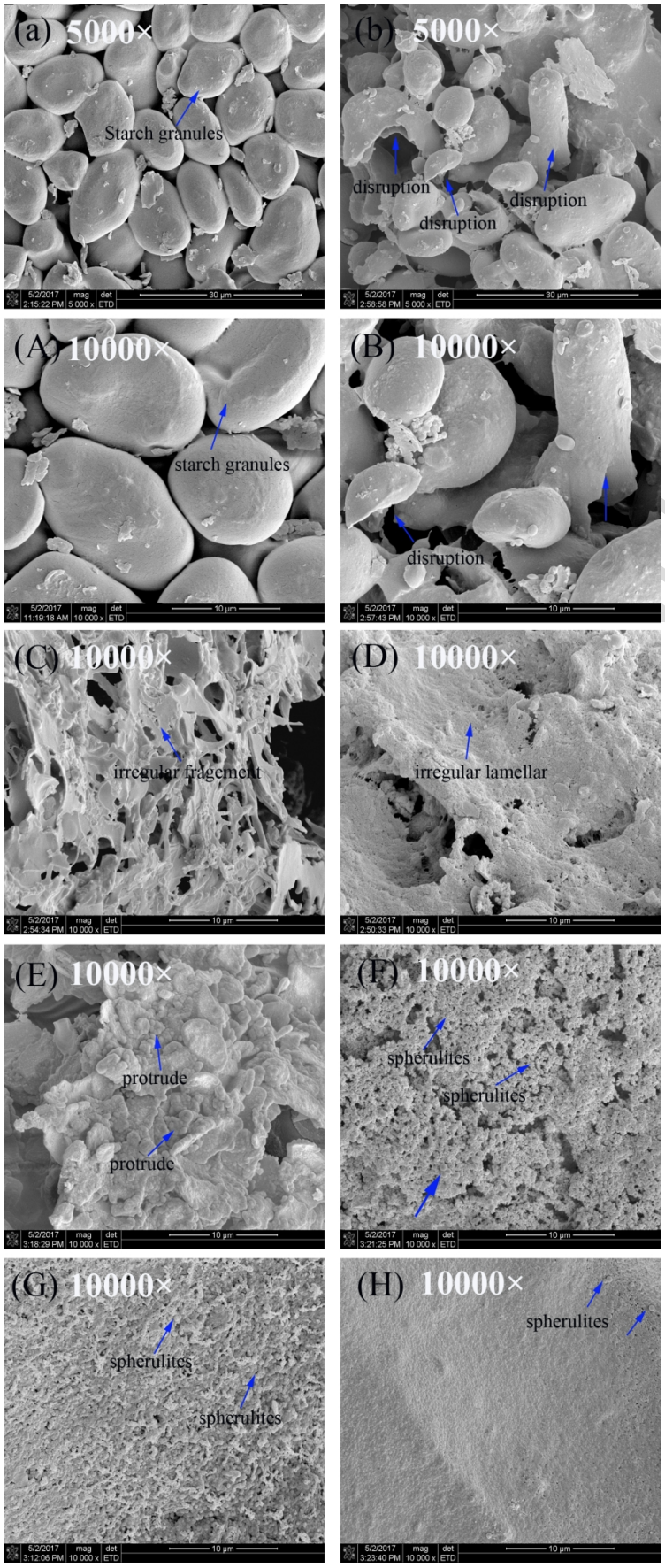

616

617 Figure 6

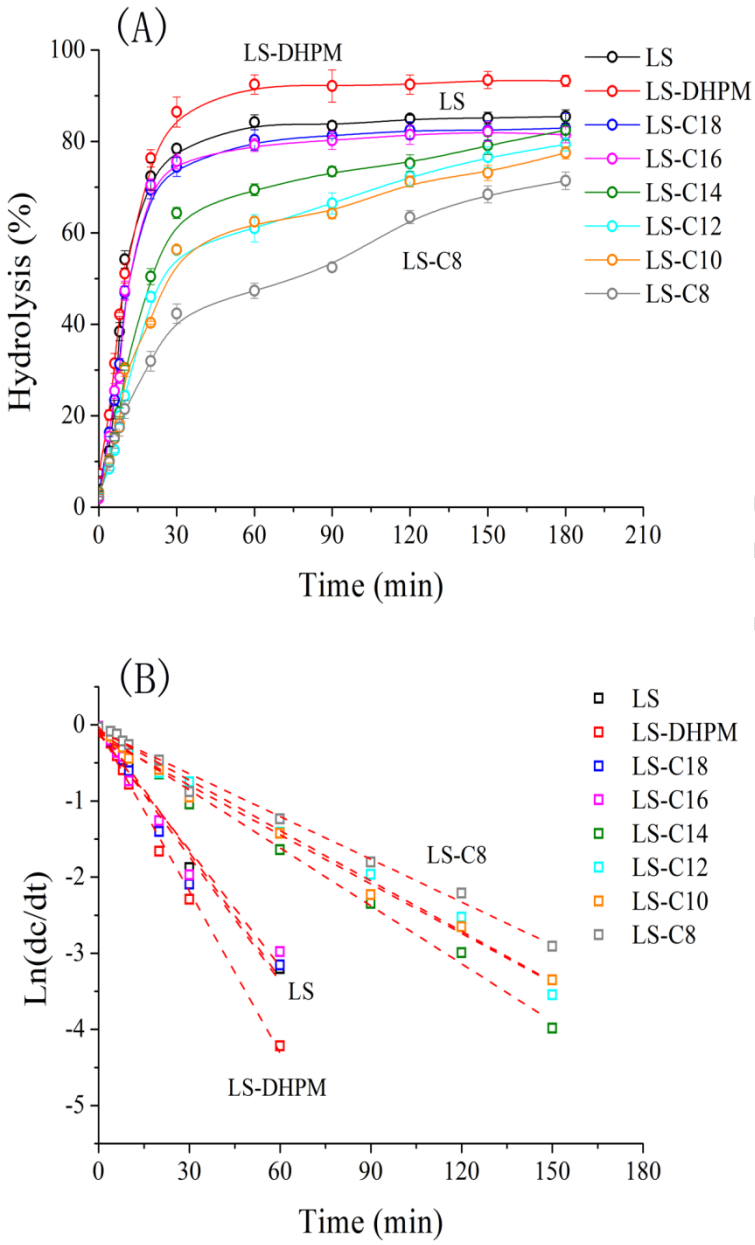

618

Highlight

- Octanoic acid was suitable to interact with lotus seed starch in microfluidization. .
- A Strong V_{6I}-type semi-crystalline was observed in starch-octanoic acid complex
- The complexes had more spherocrystals with decreasing fatty acids chain length.
- The digestibility was depended on semi-crystalline structure of complexes